A Transition Arm Modular Multilevel Universal Pulse-Waveform Generator for Electroporation Applications

Mohamed A. Elgenedy, *Student Member, IEEE*, Ahmed Darwish, Shehab Ahmed, *Senior Member, IEEE*, and Barry W. Williams

***Abstract*—High-voltage (HV) pulses are used in electroporation to subject pulsed electric field (PEF) onto a sample under treatment. Pulse-waveform shape, voltage magnitude, pulse duration, and pulse repetition rate are the basic controllable variables required for particular PEF application. In practice, a custom-made pulse generator is dedicated for each PEF application with limited flexibility in changing these variables. In this paper, a universal pulse-waveform generator (UPG) is proposed, where the controller software algorithm can manipulate a basic generated multilevel pulse waveform to emulate many different PEF pulse waveforms. The commonly used PEF HV pulse waveforms can be generated as bipolar or monopolar with controllable pulse durations, repetition times, and voltage magnitudes. The UPG has the ability to generate multilevel pulses that have controllable dv/dt, which allows reduction of the electromagnetic interference generated by the converter. The UPG topology is based on half-bridge modular multilevel converter (HB-MMC) cells forming two transition arms in conjunction with two bistate arms, together creating an H-bridge. The HB-MMC cell capacitors provide a controllable energy source which charge from the dc input supply and discharge across the load, while the two bistate arms allow charging the HB-MMC cell capacitors. Hence, the UPG topology offers modularity, redundancy, and scalability. The HB-MMC individual cell capacitance is low and the cell voltages are balanced by employing the sorting and rotating algorithm used in conventional HB-MMC topologies for HV dc transmission applications. The viability of the proposed UPG converter is validated by MATLAB/Simulink simulation and scaled-down experimentation.**

***Index Terms*—Electroporation, high voltage (HV), modular multilevel converters (MMCs), pulsed electric field (PEF), pulse-waveform generator, series-connected insulated-gate bipolar transistors (IGBTs), transition arm.**

Manuscript received June 16, 2016; revised September 18, 2016 and November 8, 2016; accepted January 3, 2017. Date of publication January 16, 2017; date of current version August 2, 2017. This work was supported by the Qatar National Research Fund (a member of the Qatar Foundation) under National Priorities Research Program Grant 7-203-2-097. The statements made herein are solely the responsibility of the authors. Recommended for publication by Associate Editor M. Tavakoli Bina.

M. A. Elgenedy is with the Department of Electronic and Electrical Engineering, University of Strathclyde, Glasgow G1 1RD, U.K., and also with the Department of Electrical Engineering, Faculty of Engineering Alexandria University, Alexandria 21544, Egypt (e-mail: m.atef.elgenedy@gmail.com).

A. Darwish and B. W. Williams are with the Department of Electronic and Electrical Engineering, University of Strathclyde, Glasgow G1 1XQ, U.K. (e-mail: ahmed.mohamed-darwish-badawy@strath.ac.uk; B.W.Williams@eee.strath.ac.uk).

S. Ahmed is with the Department of Electrical and Computer Engineering, Texas A&M University at Qatar, Doha 23874, Qatar (e-mail: shehab.ahmed@qatar.tamu.edu).

Color versions of one or more of the figures in this paper are available online at http://ieeexplore.ieee.org.

Digital Object Identifier 10.1109/TPEL.2017.2653243

I. Introduction

ELECTROPORATION is the process where a biological cell membrane is exposed to a specific pulsed electric field (PEF) [1]. Depending on the biological cell characteristics, a suitable PEF can be applied for electroporation [2]. Typically, there are two types of electroporation, namely reversible and irreversible. In reversible electroporation, the cell membrane survives after the electroporation process. This is required, for example, when inserting protein cells in the cell membrane [3]. However, death of the microorganism's cell is associated with irreversible electroporation [3]. Water treatment, air pollution control, and food sterilization are examples, where irreversible electroporation is exploited for either decontamination or sterilization from bacteria and harmful microorganisms using PEF [4]–[7].

Generating the electroporation pulses is primarily controlled by the applied high voltage (HV) across the cell membrane, pulse-waveform shape, and pulse application time. Therefore, there is a wide range of pulses, where a specific pulse suites a specific application. Accordingly, the voltage magnitude can be in the kilovolt range (1–100 kV), while the pulse duration ranges between nanoseconds and milliseconds [8]. Generally, the higher the voltage, the shorter the pulse duration.

Among the wide range of possible HV pulse waveforms for electroporation, rectangular, exponential, and combined narrow and wide pulse duration pulses are commonly used, as shown in Fig. 1 [8]. The HV pulses can be either monopolar or bipolar, as shown in Fig. 1. The rectangular pulses [see Fig. 1(a) and (d)] and the exponential pulses [see Fig. 1(b) and (e)] are usually applied in water and air disinfection applications [9]. The pulses of combined narrow and wide pulse durations, shown in Fig. 1(c) and (f), are recently proposed in [1], [5], and [10] and are preferred in safe food sterilization, without altering the food nutrition values and freshness quality [11], [12].

Marx generators, pulse forming networks, and Blumlein lines are commonly used classical generators to generate electroporation HV pulses [13]–[15]. However, with ongoing HV semiconductor switch development (in silicon and silicon carbide), mainly increased voltage rating and high-switching-frequency

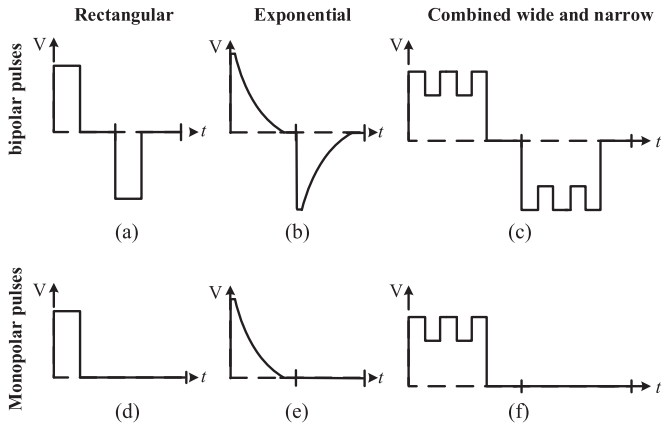

Fig. 1. Commonly used pulse waveforms in electroporation.

capability, it is possible to generate the necessary HV pulses via power-electronics-based converters [16].

In a solid-state Marx generator, as an example, the semiconductor switches operate to control the charging and discharging of its capacitors such that they charge in parallel and then discharge in series across the load [17]–[19]. The modular buck–boost converters in [20] generate HV pulses with proper turn ON/OFF operation of the semiconductor switches. Half-bridge modular multilevel converter (HB-MMC) cells are used in [21] to generate HV pulses from a low-voltage supply by charging the cell capacitors sequentially, which are then discharged in series across the load. Modified HB-MMC cells are used in [22] and [23], as one phase leg of the three-phase HB-MMC topologies used for high-voltage dc (HVDC) application, to generate HV pulses from an HVDC supply. A series diode between adjacent cells modification affords sensorless operation of the MMC cell voltages, when employing a specific ON/OFF switching sequence.

Neither classical nor modern semiconductor-based pulse generators can generate different pulse waveforms when utilizing one converter topology. Therefore, usually, there is a specific pulse generator for every associated PEF application, to generate its required pulses. Also, for a given pulse waveform, some generators can only generate either monopolar or bipolar polarity pulses [24]. Series-connected HV switches for chopping the HVDC supply to form the pulses, adopted in [18], [19], and [25], for example, are evident. Similarly, in [21], HV series-connected diodes are required to bypass the load during cell-capacitor charging.

This paper proposes a universal HV pulse-waveform generator (UPG) fed from HVDC supply, V_s, where the UPG is based on series-connected HB-MMC cells forming two transition arms and two bistate arms, together forming an H-bridge. The transition arm cell capacitors provide a controllable energy source, which allow multilevel voltage transitions. The bistate arms facilitate the charging of the HB-MMC cell capacitors in the transition arms from V_s after discharging across the load. The transition arm concept was introduced in [26] for dual-active-bridge (DAB) application in HVDC transmission, in which the transition arm allows multilevel voltage transition between positive and negative voltage rails creating a quasi-two-level voltage waveform with reduced dv/dt in order to reduce the voltage stresses on the DAB ac transformer. However, in this paper, the two transition arms are utilized to build bipolar multilevel pulse waveforms such that one arm allow multilevel voltage transition between 0 and $+V_s$, while the multilevel voltage transition in the other arm is between 0 and $-V_s$.

Without changing any physical connections, by only changing the controller software algorithm, the UPG is able to generate a multilevel pulse waveform that has controlled dv/dt, which allows reduction of the electromagnetic interference (EMI) generated by the converter [27]. Such a feature allows the generation of the basic HV pulses, namely rectangular, exponential, as well as combined narrow and wide pulse waveforms. Also, not only can bipolar or monopolar pulses be generated, but pulse waveforms with special characteristics are also possible. For example, the proposed topology facilitates changing the duration of a particular polarity or merging both polarities null durations. Therefore, the UPG can be used in both reversible and irreversible electroporation applications.

Utilizing the HB-MMC cells and the bistate arms in the UPG affords output flexibility by software control, along with hardware modularity, scalability, and redundancy. Each UPG HB-MMC cell capacitance is low, which dramatically reduces converter cost, footprint, and weight. Individual cell voltages are balanced with the conventional sorting algorithm used in HB-MMC topologies for HVDC transmission applications, where cell capacitors are continuously rotated and sequenced based on measurement of their individual voltage [28], [29]. Although each bistate arm is formed by a series connection of insulated-gate bipolar transistors (IGBTs), the IGBTs are turned ON/OFF only when the voltage across the arm is zero, zero-voltage switching (ZVS) (or, near to zero). Transitional voltage sharing occurs with zero IGBT current; thus, voltage sharing normally associated with hard-switched series-connected semiconductors is not an issue.

The proposed UPG converter is introduced in Section II, and its operation principle is outlined in Section III. Its analysis and parameters selection are given in Section IV. Simulation and experimental results are present in Sections V and VI, respectively, and the proposed UPG topology variations and limitations are discussed in Section VII.

II. UPG Converter Topology

The proposed UPG converter topology is shown in Fig. 2. It consists of four arms forming an H-bridge; the two upper arms, Arm1 and Arm2, are the transition arms formed of N series-connected HB-MMC cells, while the two lower arms, Arm3 and Arm4, are the bistate arms formed of series-connected IGBT switches. Each transition arm has a small arm series inductor L_a to supress the inrush current between cell capacitors during their insertion process and to allow cell-capacitor charging when connected to the dc input supply V_s.

Any HB-MMC cell of the transition arms has a capacitor C_c in series with an auxiliary IGBT switch/diode T_x and both

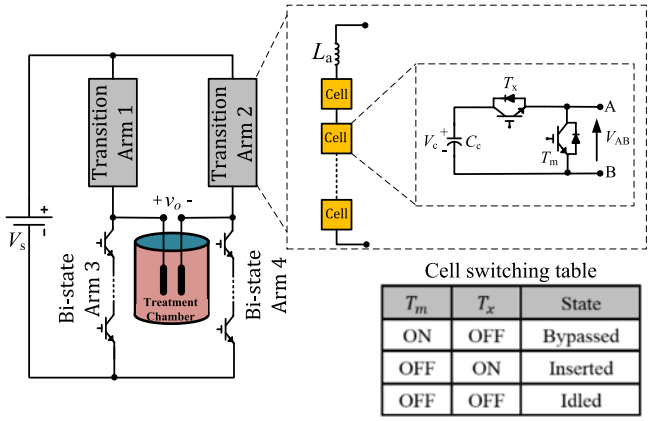

T_m	T_x	State
ON	OFF	Bypassed
OFF	ON	Inserted
OFF	OFF	Idled

Fig. 2. Proposed UPG converter topology.

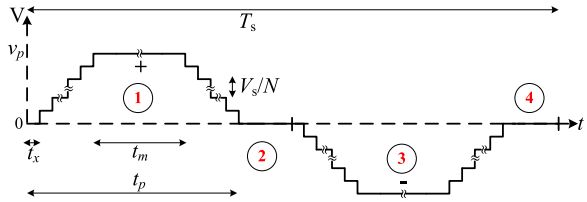

Fig. 3. UPG basic multilevel pulse waveform, where $Nt_x \ll t_m$.

are paralleled to a main IGBT switch/diode T_m, as shown in Fig. 2. Each cell can operate in any of three switch states, bypass, insertion, and idle, as shown in Fig. 2. The bypass state (when the main IGBT is ON and the auxiliary IGBT is OFF) implies that the cell is a short circuit and the voltage across the cell terminal $V_{\rm AB}$ is near zero. The insertion state (when the main IGBT is OFF and the auxiliary IGBT is ON) connects the cell capacitor to $V_{\rm AB}$; hence, the cell voltage is $V_{\rm AB} = V_c$. The idle state (when both the main and auxiliary IGBTs are OFF) introduces an open circuit across the cell terminal at steady state, thus hindering the current flow through the arm from the dc link. Therefore, the two transition arms have tristate modes. Since the two lower arms are formed from series-connected IGBTs, they can operate only in bistate modes (either turned ON or OFF).

For proper UPG converter operation, each arm must be able to withstand the dc-link voltage V_s. Consequently, the voltage of the HB-MMC cell capacitors in the transition arm should be balanced, and each cell voltage fluctuates around V_s/N. The MMC sorting and rotating technique in [28] is adopted. Therefore, each cell voltage is continuously measured, compared with other cell voltages in that corresponding arm, and the capacitor voltages are sorted. Accordingly, the highest voltage capacitor among the available capacitors is inserted first at each voltage level during the transition from 0 to $\pm V_s$, while the lowest cell voltage is bypassed first during the transition from $\pm V_s$ to 0.

The UPG basic multilevel pulse waveform V_p is shown in Fig. 3 and can be defined by four sequential intervals: positive pulse, positive null, negative pulse, and negative null. Controlling the five parameters defining this basic waveform allows the generation of any desired pulse waveform, like the waveforms

TABLE I
GENERATION OF DIFFERENT PULSE WAVEFORMS FROM THE BASIC UPG MULTILEVEL PULSE WAVEFORM

Waveform		Controlling attributes
Rectangular Pulse	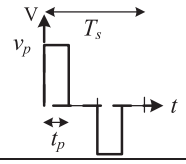	By setting $t_p = t_m$ and $t_x = 0$, accordingly all the corresponding arm cells will operate simultaneously.
Exponential Pulse	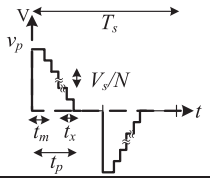	By inserting all corresponding cell-capacitors for duration t_m, then bypassing them one by one gradually to reduce the voltage to zero in Nt_x, hence $t_p = t_m + Nt_x$.
Combined Narrow and Wide Pulse Durations	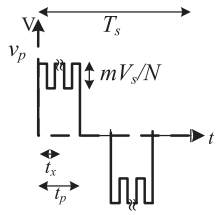	By setting t_p as the wide pulses duration with an amplitude of V_s, and the narrow pulses of magnitude $(V_s - mV_s/N)$ and duration t_x. Where m is the number of bypassed cells in the corresponding arm.

in Fig. 1. The five parameters are repetition time T_s, total pulse time t_p, pulse plateau time t_m, cell voltage step V_s/N, and step voltage-level applied time t_x. Accordingly, there are $N+1$ voltage levels from the zero-voltage level to the peak pulse voltage V_s (neglecting IGBT ON resistances, diode voltage drops, and arm inductor resistance). The positive and the positive null intervals in the UPG basic waveform (regions 1 and 2 in Fig. 3, respectively) can be expressed mathematically as

$$v_p = \begin{cases} \sum_{n=1}^{N} \dfrac{n}{N} V_s, & 0 \le t < Nt_x \\ V_s, & Nt_x \le t < (Nt_x + t_m) \\ \sum_{n=1}^{N} \left(1 - \dfrac{n}{N}\right) V_s, & (Nt_x + t_m) \le t < t_p \\ 0, & t_p \le t < {}^1\!/_2 T_s. \end{cases} \quad (1)$$

Mathematically, region 3 is the negative equivalent of region 1, while region 4 is similar to region 2. Accordingly, Table I defines the emulated pulse waveforms of Fig. 1 generated by the UPG from its basic pulse-waveform controlling attributes.

III. UPG OPERATION PRINCIPLE

The UPG generated pulse waveforms are normally bipolar, where the HB-MMC cells in Arm2 are responsible of generating the positive pulse duration, while the HB-MMC cells in Arm1 are responsible for generating the negative pulse duration. Disabling a specific transition arm will lead to generating monopolar pulse waveforms with the desired polarity.

As discussed, there are four intervals for a bipolar pulse-waveform generation cycle. The operation for each interval is shown in Table II and can be explained as follows: during the positive pulse generation interval, the two bistate arms are OFF, transition Arm1 cells are bypassed, and transition Arm2 cells are inserted.

TABLE II
OPERATING PRINCIPLE OF THE UPG

	Circuit configuration	Sequence of operation
Positive Pulse	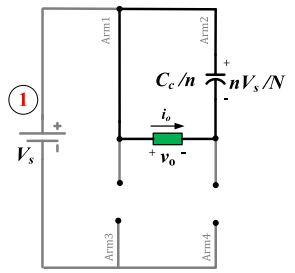	• The bi-state arms are turned OFF. • Transition Arm1 cells are bypassed to provide a path for transition Arm2 discharging cell-capacitors. • Transition Arm2 cells are inserted according to the desired pulse-waveform. • A positive pulse is formed across the load.
Positive Null	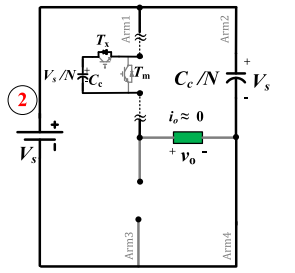	• The bi-state arms are kept OFF. • All transition Arm2 cell-capacitors are inserted while transition Arm1 is put in idle state. • The bi-state Arm4 is turned ON, keeping Arm3 OFF. • Charging the series connected cell-capacitors to the supply voltage. • The bi-state Arm4 is turned OFF.
Negative Pulse	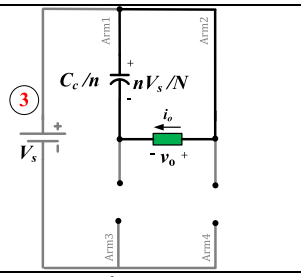	• The bi-state arms are kept OFF. • Transition Arm2 cells are bypassed to provide a path for transition Arm1 discharging cell-capacitors. • Transition Arm1 cells are inserted according to the desired pulse-waveform. • A negative pulse is formed across the load.
Negative Null	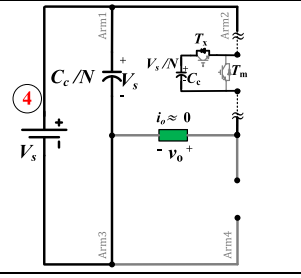	• The bi-state arms are kept OFF. • Transition Arm1 cell-capacitors are inserted while transition Arm2 is put in idle state. • The bi-state Arm3 is turned ON, keeping Arm4 OFF. • Charging the series connected cell-capacitors to the supply voltage. • The bi-state Arm3 is turned OFF.

Consequently, the equivalent series-connected capacitor C_c/n is inserted across the load producing a voltage of $+nV_s/N$, where n is the number of the inserted cells. Similarly, for negative pulse generation, again, the two bistate arms are OFF, transition Arm2 cells are bypassed, and transition Arm1 cells are inserted. Hence, the series-connected capacitor C_c/n is inserted across the load-producing voltage $-nV_s/N$. During the null intervals, Arm2 or Arm1, for positive or negative pulses, respectively, cell capacitors are charged from the dc-link supply, while the load voltage is nullified. Thus, the equivalent inserted capacitor C_c/N charges to V_s. Turning ON/OFF the bistate arms is assured soft-switching operation, ZVS (that is, the series-connected switches are switched only when the voltage across the arm is near zero). After the positive/negative pulse interval, charging of Arm2/Arm1 is the next interval that requires turning ON the bistate Arm4/Arm3.

Thus, during charging of one of the transition arms, the other transition arm is idled, and the charging cell capacitors are inserted. Therefore, the voltage across the corresponding bistate arm remains close to zero; hence, it can be turned ON allowing the input supply to charge the cells. During the charging interval, the charging transition arm voltage reaches the supply voltage V_s; hence, the voltage difference across the corresponding bistate arm is zero, and therefore, the bistate arm can be turned OFF, in a ZVS state.

Idling one transition arm during the null intervals (or, the charging interval of the other transition arms) will not prevent charging its capacitor cells, through T_x diode, when starting the converter. At the steady state, the idled arm cell-capacitor voltages are charged to the supply voltage V_s, and since they are not participating in the pulse generation, the arm voltage will not change; hence, the idled arm can be viewed as an open circuit during charging of the other transition arm, as shown in Table II.

IV. PARAMETERS SELECTION OF THE UPG

Since bipolar rectangular pulse waveform represents the case in which all the cell capacitors in the transition arms (Arm1 and Arm2) are to be inserted, giving a step from the zero-voltage level to the $\pm V_s$ voltage levels, its generation will be considered in the following analysis and cell-capacitor sizing. In this paper, HV pulses with pulse durations of microseconds or longer are considered; hence, the PEF load is modeled as a resistive load R [4], [30].

The UPG operation for each pulse polarity can be illustrated from an energy conversion perspective. Assume the individual cell capacitors are precharged to V_s/N. During the positive pulse interval, some of the energy stored in Arm2 capacitors is transferred to the load during pulse generation time t_p. Hence, Arm2 capacitors partially discharge and their voltage reduces accordingly. This energy reduction is compensated by recharging Arm2 individual cell capacitors to V_s/N during the positive null interval. These two processes are illustrated in Fig. 4. The same procedures occur during the negative pulse interval through Arm1 cell capacitors. Therefore, the energy is transferred from the input dc supply to the load in two stages: First, the input dc supply charges the corresponding cell capacitors; then, the charged cell capacitors partially discharge into the load. The energy transferred to the load E_L during the pulse time is

$$E_L = P_L t_p \tag{2}$$

where P_L is the power consumed by the load R during pulse time t_p, which can be expressed as

$$P_L = \frac{V_o^2}{R} \tag{3}$$

where V_o is the load rms voltage, which can be calculated from Fig. 4 as

$$V_o = \sqrt{\frac{1}{T_s}\int_0^{T_s} v_o^2(t)\,dt}. \tag{4}$$

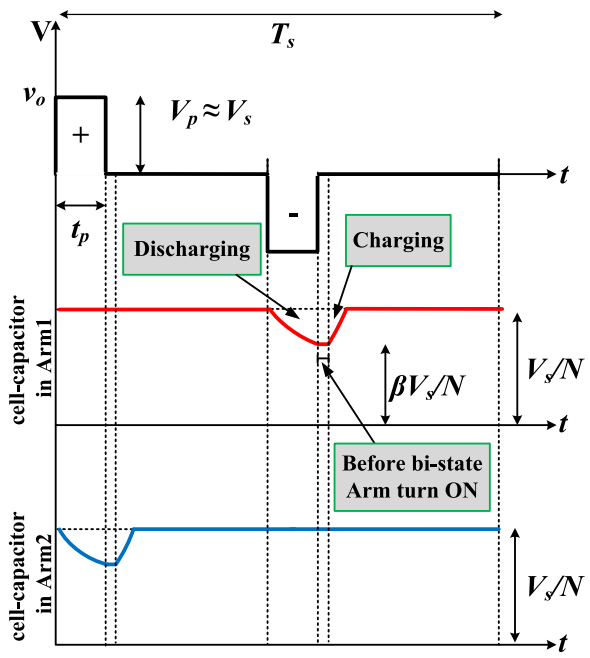

Fig. 4. Individual cell capacitors of Arm1 and Arm2 charging and discharging sequence for generating a rectangular bipolar pulse.

Thus

$$V_o = \sqrt{\frac{2t_p}{T_s}} V_p. \tag{5}$$

Neglecting IGBT voltage drops and the internal resistance of L_a, $V_p \cong V_s$; hence, the load energy per pulse polarity is

$$E_L = \frac{t_p^2 V_s^2}{T_s R}. \tag{6}$$

The energy transferred to the load is equal to the difference between the initial energy stored in the individual arm capacitors ($E^i_{\text{cell}} = \frac{1}{2} C_c \frac{V_s^2}{N^2}$) and the energy remaining after the pulse ($E^p_{\text{cell}} = \frac{1}{2} C_c \frac{\beta^2 V_s^2}{N^2}$). This energy can be estimated as

$$\Delta E_{\text{cell}} = E^i_{\text{cell}} - E^p_{\text{cell}}. \tag{7}$$

Hence

$$\Delta E_{\text{cell}} = \tfrac{1}{2} C_c \frac{V_s^2}{N^2} - \tfrac{1}{2} C_c \frac{\beta^2 V_s^2}{N^2} \tag{8}$$

where ΔE_{cell} is the energy difference in the individual cell capacitor in the discharging arm, and the cell voltage after discharge is expressed as a per unit, β, in terms of the initial cell voltage V_s/N, as shown in Fig. 4. Thus, the energy difference in the discharging transition arm of N series cells is

$$\Delta E_{\text{Arm}} = N \times \Delta E_{\text{cell}} = \tfrac{1}{2} C_c \frac{\left(1-\beta^2\right) V_s^2}{N} \tag{9}$$

where ΔE_{Arm} is the energy difference in the arm corresponding to a specific pulse polarity. Neglecting semiconductor losses, $\Delta E_{\text{Arm}} = E_L$; hence, the cell capacitance is

$$C_c = \frac{2t_p^2 N}{\left(1-\beta^2\right) T_s R}. \tag{10}$$

Denoting $\delta = t_p/T_s$, the pulse on-state duty ratio, (10) yields

$$C_c = \frac{2N\delta t_p}{\left(1-\beta^2\right) R} \alpha \tag{11}$$

where $\alpha > 1$ is a safety factor to account for neglected losses. C_c can be tailored to produce an acceptable pulse droop for a given load and pulse characteristic (increase C_c to decrease the voltage droop). The cell capacitor per unit voltage droop, $(1-\beta)$, specifies the efficiency of the resonate recharging of the cell capacitors. The resonant losses, related to the throughput power, are approximately the per unit droop, squared, viz. $(1-\beta)^2$. For example, with 10% capacitor voltage droop, the recharging losses are 1% of the average power of the pulse causing the droop. These losses are dissipated in the charging circuit resistance and the bistate arm devices as on-state losses. These device losses are mitigated by the fact that the bistate arm devices do not incur switching losses; their switching is at zero voltage, ZVS.

Consequently, the total average power P_{tot} associated with the applied HV pulses with repetition frequency f_s can be calculated in (12) for bipolar pulses, while the value is halved for monopolar pulses

$$P_{\text{tot}} = \frac{2t_p^2 V_s^2}{R} f_s^2. \tag{12}$$

The arm inductor L_a in series with the MMC cells in HVDC applications has two functions: suppressing the circulating current in the cells and limiting the dc short-circuit current [29]. Although the proposed UPG converter topology adopts the technology of an MMC-HVDC converter, the operating principle is different, and dc-link short-circuit blocking is not applicable. But small arm inductance is preferred in each transition arm (Arm1 and Arm2) such that the inrush current is suppressed when inserting the cells in series across the load during discharging or across the dc supply during charging. Additionally, resonance between L_a and the arm capacitors should be avoided [30]. Hence, the device switching frequency should be well away from the resonance frequency of the equivalent LC circuit to avoid exciting resonance currents. Therefore, based on the designed equivalent arm capacitance and repetition time, an estimation of the inductance of L_a is

$$L_a < \frac{NT_s^2}{4\pi^2 C_c}. \tag{13}$$

V. Simulation Results

The proposed UPG is assessed using MATLAB/Simulink simulations, with the parameters in Table III. The cell capacitance C_c is calculated based on (11), while (13) is used to estimate the arm inductance L_a. The number of the IGBT switches in bistate arms, Arm3 and Arm4, is $N = 10$. The simulations assess the ability of the UPG to mimic the commonly used pulse waveforms in PEF applications and the flexibility of the

TABLE III
SIMULATION SPECIFICATION

DC input voltage	V_s	10 kV
Number of cells/arm	N	10
Repetition time	T_s	200 μs
Arm inductance and resistance	L_a , r_a	2 μH, 0.1 Ω
Arm resistance	R_a	0.1 Ω
Load resistance	R	1 kΩ
Cell capacitance	C_c	5 μF
Per unit remaining capacitor voltage	β	0.95
Safety factor	α	2

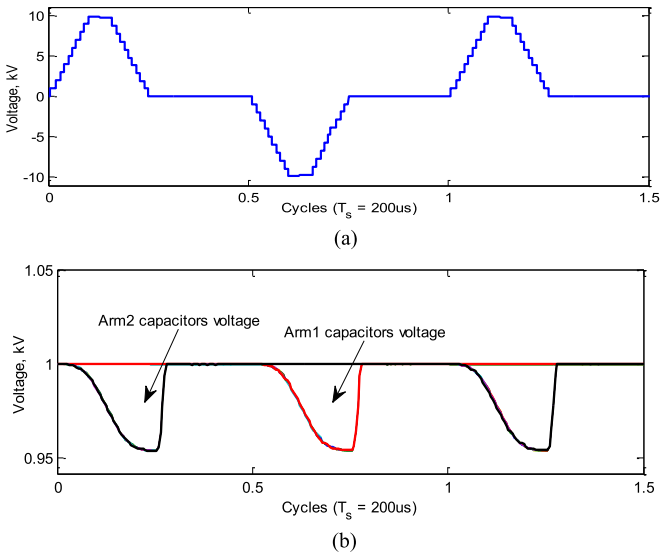

Fig. 5. Simulation of basic UPG multilevel pulse waveform. (a) Output bipolar HV pulses. (b) Arm1 and Arm2 capacitor voltages.

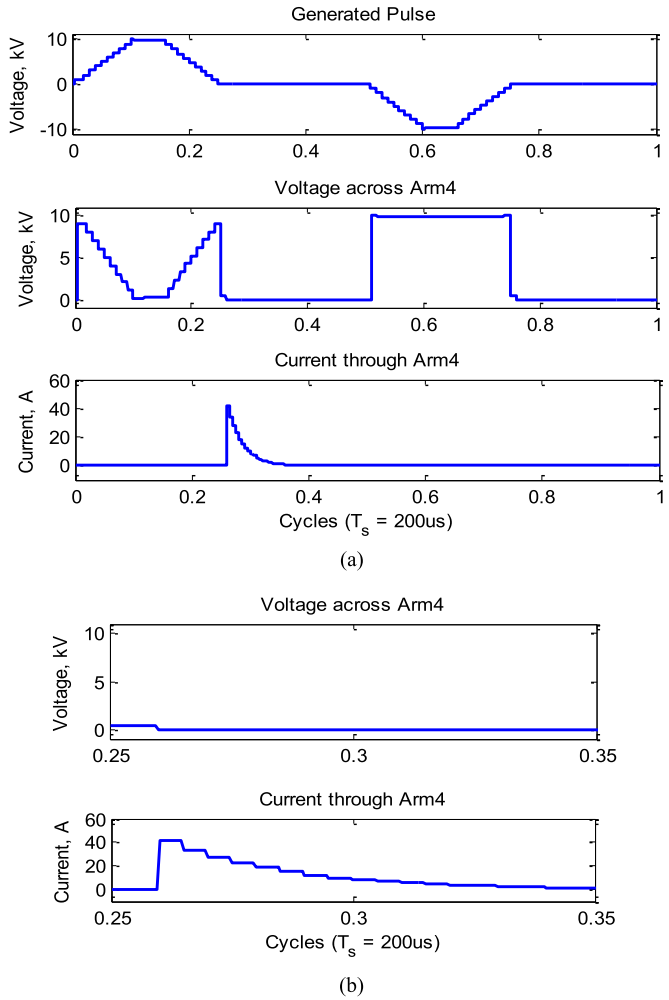

Fig. 6. Voltage across and current through bistate Arm4 during positive pulse generation via Arm2 cell capacitors (a) during one complete pulse cycle and (b) zoomed view of Arm4 voltage and current during Arm2 capacitors recharging.

converter to control the generated pulse attributes via the controller software-algorithm, without any physical changes to the power topology or the load connection.

With a repetition frequency of 5 kHz, the basic UPG multilevel pulse waveform is shown in Fig. 5. Fig. 5(a) shows the generated voltage pulse with $t_x = 2$ μs, $t_m = 14$ μs, and $t_p = 50$ μs. The cell voltages of Arm1 and Arm2 are shown in Fig. 5(b). In Fig. 5(b), Arm2 contributes to the positive pulse generation, while Arm1 contributes to the negative pulse generation. The cell capacitors charge to the 1 kV after their voltage decreases during discharge across the load. The voltage across and the current through the bistate arm Arm4 during one cycle of pulse generation are shown in Fig. 6. In Fig. 6(b), when the voltage across Arm4 is near zero, the bistate arm switches are turned ON, allowing capacitor charging current to flow. After the cell capacitors are charged, the current reaches zero, and the voltage across the bistate arm is zero; hence, the arm switches can be turned OFF. During negative pulse generation, the bistate arm is maintained OFF, and the voltage across it is V_s, as shown in Fig. 6(a).

Fig. 7(a) shows the generation of positive monopolar multilevel pulse waveform, while the negative counterpart is depicted in Fig. 7(b). Since the two transition arms can operate independently, not only a certain polarity can be omitted, but it can be generated with different characteristics. For example, in Fig. 8(a), the positive pulse is generated with $t_x = 2$ μs, $t_m = 24$ μs, and $t_p = 60$ μs, while the negative pulse is generated with $t_x = 2$ μs, $t_m = 2$ μs, and $t_p = 38$ μs. Since the positive pulse duration is longer, the decrease in the cell voltages of Arm2 is more than those for Arm1 [see Fig. 8(b)].

By setting $t_x = 0$ and $t_m = t_p = 10$ μs, in the controller software, a rectangular pulse can be generated. The simulation results of bipolar rectangular pulses are shown in Fig. 9(a). Generating positive monopolar and combined null duration rectangular pulses is explored in Fig. 9(b) and (c), respectively, with positive and negative pulse durations of 10 μs.

The features of controlled dv/dt in the basic generated multilevel pulse waveform and the conventional rectangular pulse waveform can be combined, as shown in Fig. 10(a) and (b), with a repetition frequency of 10 kHz. The exploitable lower value of t_x is limited by switching device turn ON and OFF delay times.

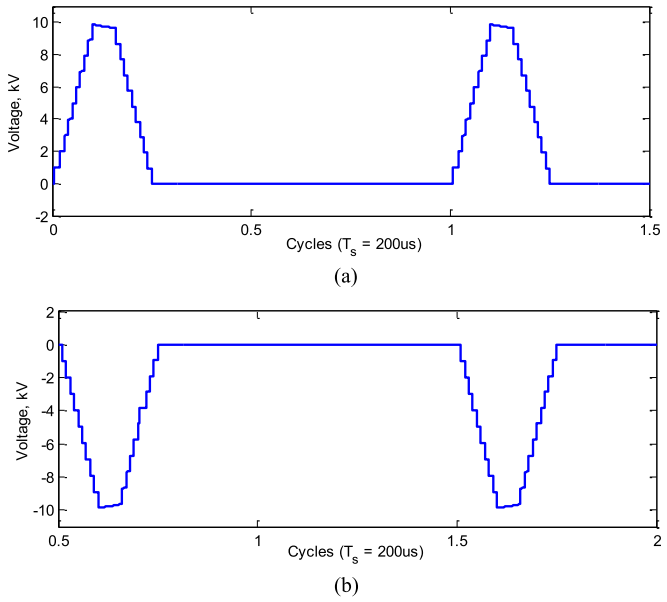

Fig. 7. Simulation of monopolar UPG multilevel pulses. (a) Positive. (b) Negative.

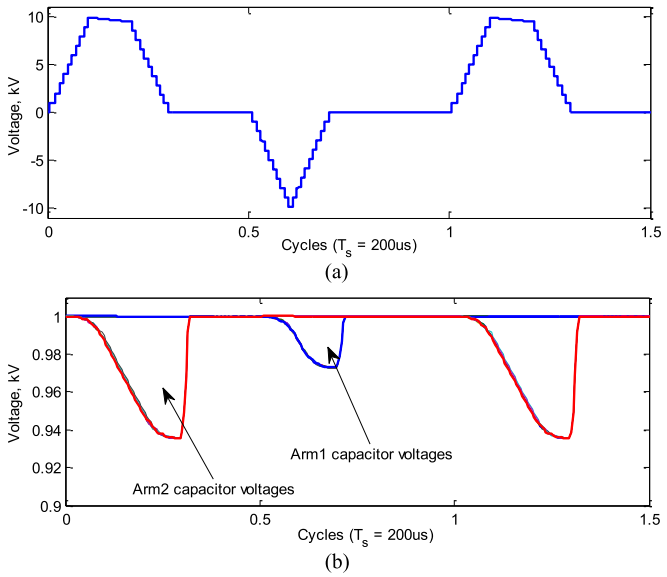

Fig. 8. Simulation of asymmetric bipolar UPG multilevel pulses. (a) Output bipolar HV pulses. (b) Arm1 and Arm2 capacitor voltages.

In Fig. 10(a), the t_x value is 0.1 μs (viable with SiC 1700-V, 45-mΩ MOSFETs, with 50-ns turn ON and OFF delays), while t_m is 5 μs; hence, the total rise time is much shorter than the plateau time. If a faster rise time is required, grouping of the cells can be employed. As shown in Fig. 10(b), to achieve a rise time of 0.3 μs, the ten cells are voltage sorted into three groups: two groups of three cells and one group of four cells.

Employing the flexibility afforded by the generated basic multilevel pulse waveform from the UPG allows generating both exponential and combined wide and narrow pulse waveforms. Such waveforms can be generated with either bipolar or monopolar polarities. With $t_x = 2$ μs and $t_m = 10$ μs,

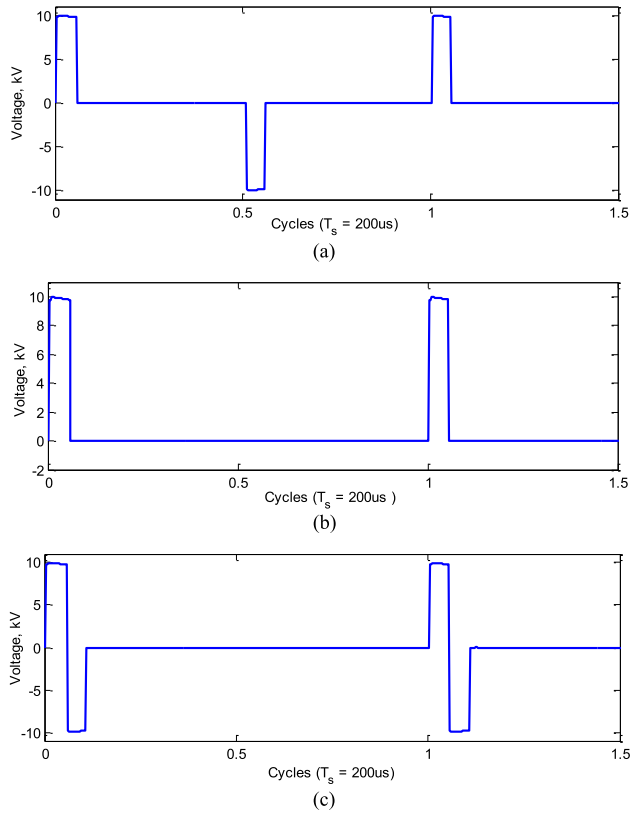

Fig. 9. Simulation of UPG rectangular output HV pulses: (a) bipolar, (b) positive monopolar, and (c) combined null durations.

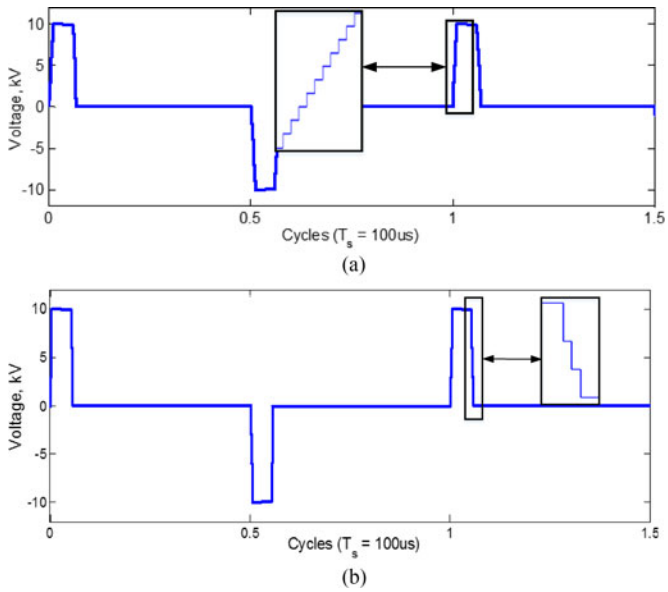

Fig. 10. Simulation of UPG 10-kHz multilevel rectangular HV pulses with $t_x = 0.1$ μs and $t_m = 5$ μs. (a) Without cells grouping. (b) With cells grouping.

Fig. 11(a) shows bipolar exponential pulses and Fig. 11(b) shows positive monopolar exponential pulses. Consequently, with $m = 5$ and $t_x = 10$ μs, bipolar combined wide and narrow pulses are shown in Fig. 12(a) and the negative monopolar version is shown in Fig. 12(b).

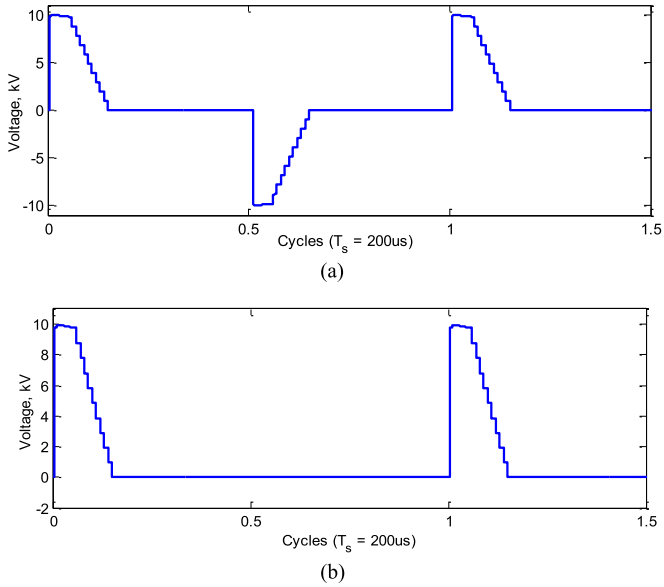

Fig. 11. Simulation of UPG exponential HV pulses with $t_x = 2\ \mu$s and $t_m = 10\ \mu$s. (a) Bipolar. (b) Positive monopolar.

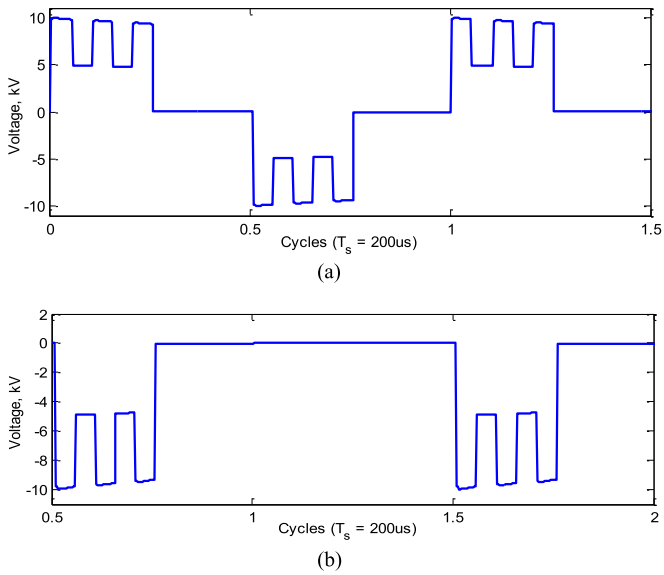

Fig. 12. Simulation of UPG combined wide and narrow HV pulses with $m = 5$ and $t_x = 10\ \mu$s. (a) Bipolar. (b) Negative monopolar.

TABLE IV
EXPERIMENTAL SPECIFICATION

DC input voltage	V_s	150 V
Number of cells/arm	N	3
Repetition frequency for bipolar pulses	$1/T_s$	1.8 kHz
Repetition frequency for monopolar pulses	$1/T_s$	3.6 kHz
Arm inductance and resistance	L_a , r_a	1 μH, 0.2 Ω
Load resistance	R	100 Ω
Cell capacitance	C_c	15 μF
Per unit remaining capacitor voltage	β	0.9
Safety factor	α	2

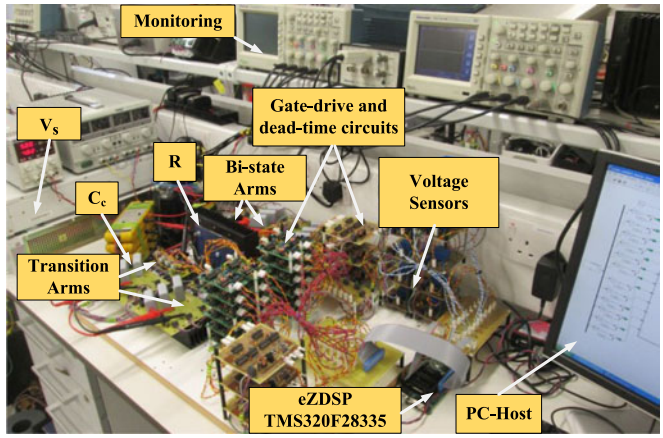

Fig. 13. Scaled-down experimental test rig.

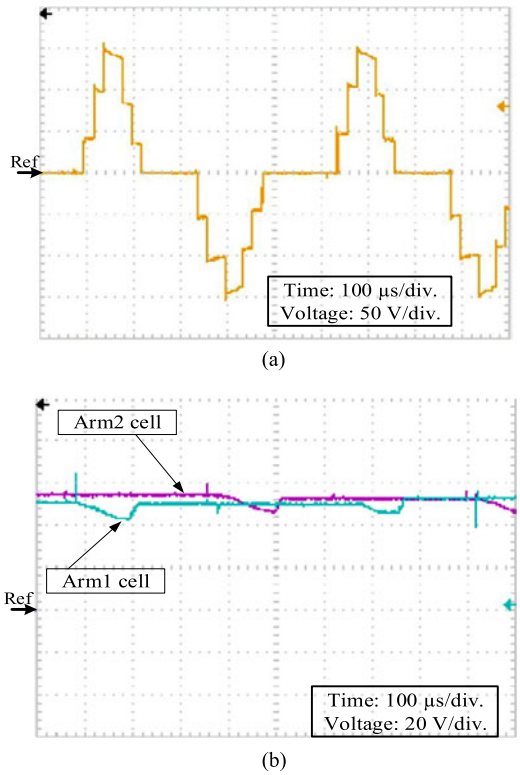

Fig. 14. Experimental results for UPG four-level bipolar pulses with a 50-V level. (a) Output pulses. (b) Cell-capacitor voltage in the two transition arms.

VI. EXPERIMENTAL RESULTS

The scaled-down UPG power circuit from Fig. 2 uses IGBT switches (STGW30NC60WD) for the HB-MMC arms that have antiparallel diodes, while the bistate arms use Infineon IGW60T120 IGBTs. The control algorithm is implemented in eZDSP, which is a digital signal processor (DSP) board based on the Texas Instruments TMS320F28335 DSP, to generate the required gating signals for the UPG switches in the four arms. The experimental specifications are given in Table IV, and the scaled-down experimental rig is shown in Fig. 13. The experimentally generated four-level basic multilevel pulse waveform is shown in Fig. 14. The output voltage pulses are shown in

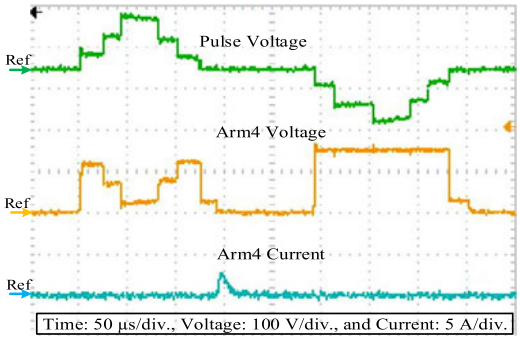

Fig. 15. Voltage across and current through bistate Arm4 during complete cycle of pulse generation via Arm2 cell capacitors.

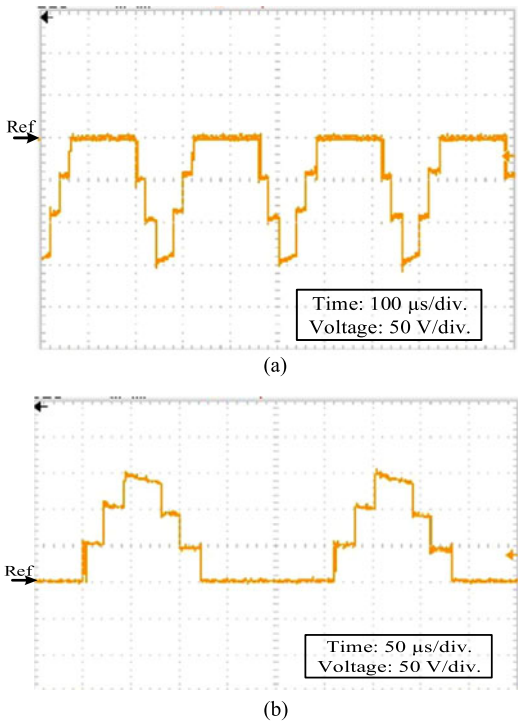

Fig. 16. Experimental results for UPG four-level monopolar pulses with a 50-V level. (a) Negative. (b) Positive.

Fig. 14(a) with $t_x = 20\ \mu$s, $t_m = 40\ \mu$s, and $t_p = 120\ \mu$s, whereas a cell-capacitor voltage from Arm1 and Arm2 are presented in Fig. 14(b). Since the input supply voltage is 150 V, the cell capacitors are charged to 50 V; then, during the associated pulse time, the corresponding transition arm capacitors discharge across the load reducing the cell-capacitor voltage to 44 V. Fig. 15 shows the waveforms of voltage across and the current through the bistate arm Arm4 during a complete cycle of the generated pulse. The waveforms reveal that the bistate arm is turned ON/OFF only when the voltage across the arm is near zero, ZVS. With $t_x = 20\ \mu$s, $t_m = 40\ \mu$s, and $t_p = 120\ \mu$s, negative plus positive monopolar four-level voltage pulses are shown in Fig. 16(a) and (b), respectively.

Generating rectangular pulses with different characteristics is explored in Fig. 17. Symmetrical rectangular bipolar pulses with

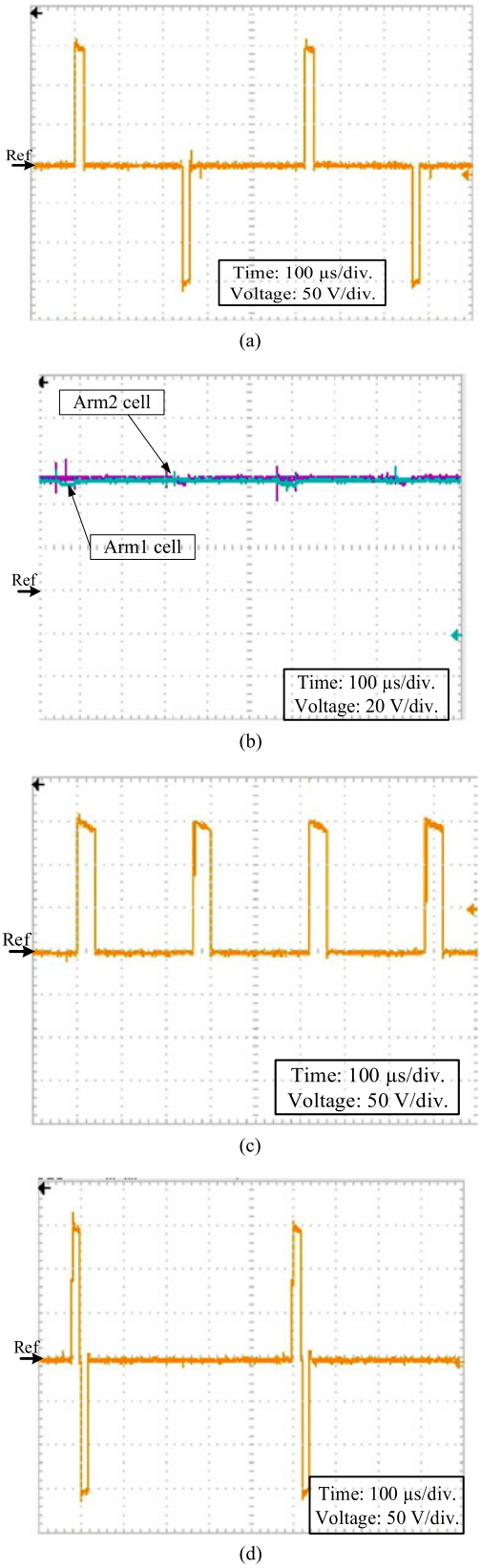

Fig. 17. Experimental results for UPG symmetrical rectangular pulses. (a) Bipolar with $t_m = 20\ \mu$s. (b) Cell-capacitor voltage in the two transition arms. (c) Positive monopolar with $t_m = 40\ \mu$s. (d) Combined null durations with $t_m = 20\ \mu$s.

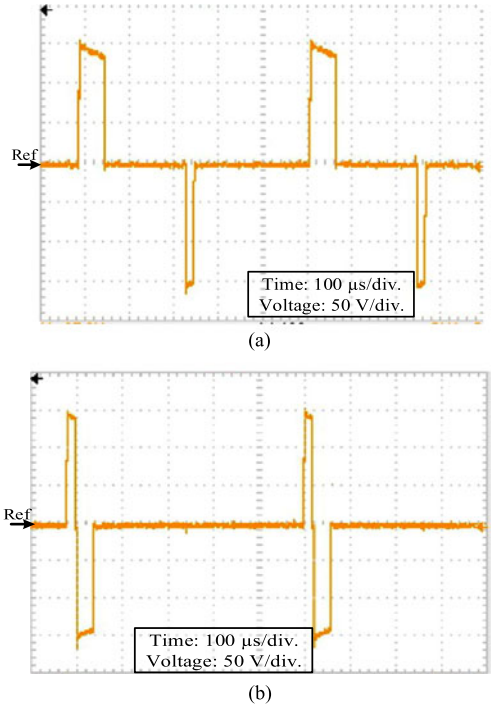

Fig. 18. Experimental results for UPG asymmetrical rectangular pulses. (a) Bipolar with positive $t_m = 40\ \mu$s and negative $t_m = 20\ \mu$s. (b) Combined null durations with positive $t_m = 20\ \mu$s and negative $t_m = 40\ \mu$s.

$t_m = 20\ \mu$s are shown in Fig. 17(a), whereas a cell-capacitor voltage from Arm1 and Arm2 is presented in Fig. 17(b). Positive monopolar pulses with $t_m = 40\ \mu$s are shown in Fig. 17(c), while combined null-duration pulses are illustrated in Fig. 17(d).

Asymmetric rectangular pulse generation is shown in Fig. 18(a) and (b). Fig. 18(a) shows a 40-μs rectangular positive pulse followed by a 20-μs negative pulse. An asymmetric combined null-duration rectangular pulse is depicted in Fig. 18(b) with pulse times of 20 and 40 μs, positive and negative, respectively.

Bipolar exponential pulses with $t_x = 20\ \mu$s and $t_m = 40\ \mu$s are shown in Fig. 19(a), and a cell-capacitor voltage in the two transition arms is shown in Fig. 19(b), while the monopolar version is shown in Fig. 19(c). The combined wide and narrow pulses with $m = 2$ and $t_x = 20\ \mu$s are shown in Fig. 20(a)–(c) for bipolar pulses, its cell-capacitor voltage in the two transition arms, and its monopolar version of pulses, respectively.

Finally, to explore the validity of the concept in generating wide range of pulses, a bipolar rectangular pulse of duration of 4 μs is generated with a repetition rate of 10 kHz and a voltage of 0.6 kV peak–peak, as shown in Fig. 21.

It should be noted that the series-connected IGBTs in the bistate arms, although in an OFF state during rail-to-rail transitions, require shunt-connected voltage-sharing resistors and parallel capacitors to account for static leakage and output capacitance variation between series devices.

VII. Topology Variations and Limitations

There are UPG topology variations, dependent on the application requirements.

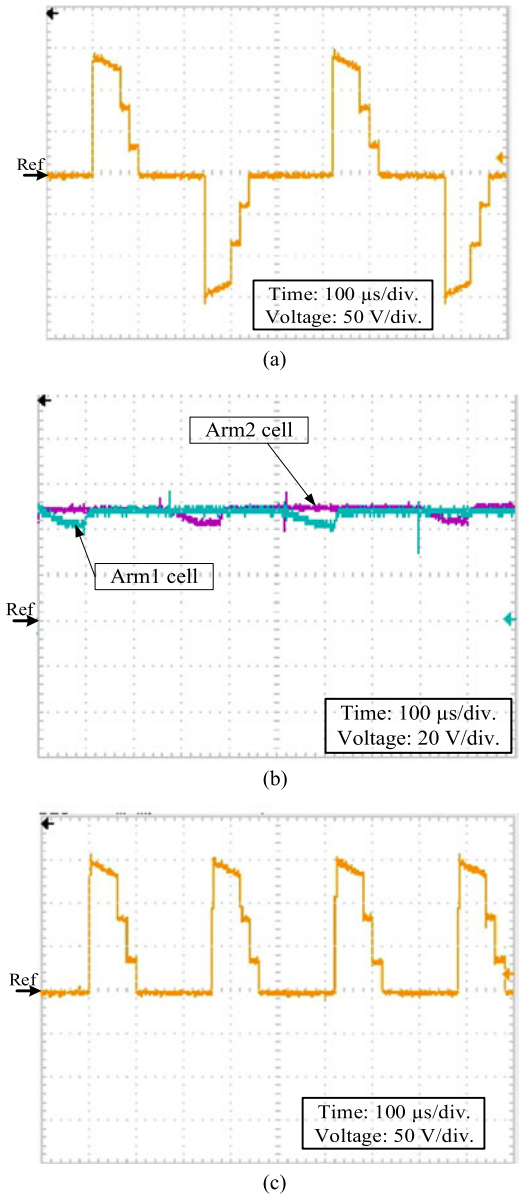

Fig. 19. Experimental results for UPG exponential pulses with $t_x = 20\ \mu$s and $t_m = 40\ \mu$s. (a) Bipolar. (b) Cell-capacitor voltage in the two transition arms. (c) Monopolar.

1) *Arm inductance*: The arm inductor L_a is small and may be accounted for by the inherent internal wiring and connection of the cells. Clamping the inductors with freewheel diodes is possible, but the low voltage of the forward-biased diode may result in an excessively long L/R reset time constant, which will limit the upper operating frequency. The energy of remaining unclamped stray inductance rings with the cell capacitors.
2) *Elimination of bistate arm diodes*: MMC cell-capacitor recharging involves an *LCR* oscillation, where, if underdamped, the current alternately reverses. The damping losses are independent of the circuit Q; thus, critical damping incurs the lowest stresses, with an acceptable settling time. As such, without current reversal, the bistate

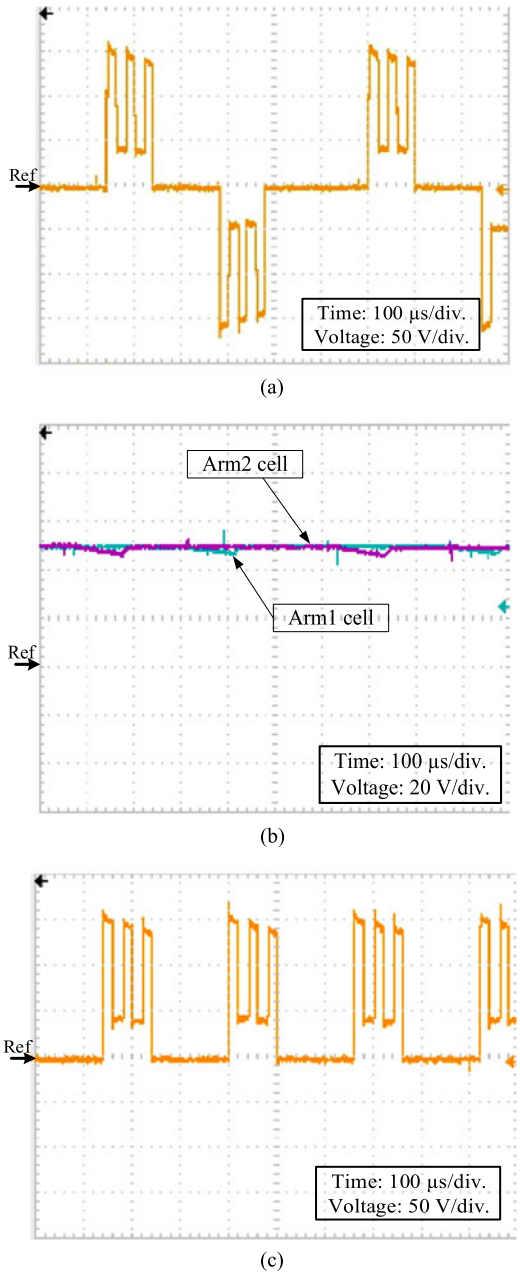

Fig. 20. Experimental results for UPG combined wide and narrow pulses with $m = 2$ and $t_x = 20$ μs. (a) Bipolar. (b) Cell-capacitor voltage in the two transition arms. (c) Monopolar.

arm diodes across the IGBTs are redundant. To maximize power transfer, any (added and/or exiting) resistance should be in the bistate arm. Both MMC arm series inductors can be moved to their associated series bistate arm.

3) *Bistate arm switches*: The switching properties of the bistate arm devices can be much slower than those necessary for the transition arms (HB-MMC arms). Also, because their inter-dc rail state transitions are with zero current, they can be higher voltage (consequently slower) rated devices, used near their voltage limit. Thus, the number of bistate arm series-connected devices can be much less than N, the number MMC cells. The tradeoff of higher voltage devices is higher OFF-state leakage current, so the parallel-connected static voltage-sharing resistance is decreased.

4) *The input supply voltage*: The proposed UPG topology for generating the HV pulses can be supplied from a dc–dc boosting stage. Additionally, the use of a 12-pulse ac–dc thyristor half-controlled converter to supply the UPG offers soft start up and shut down.

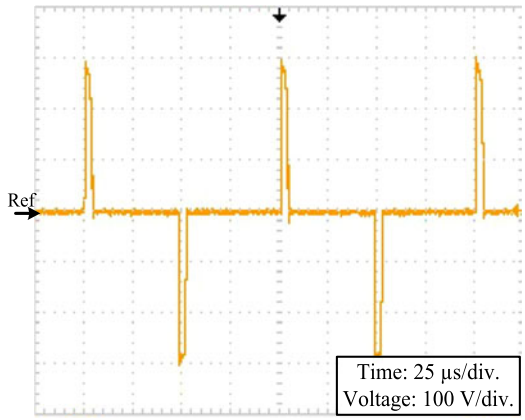

Fig. 21. Experimental results for UPG bipolar rectangular pulses with $t_m = 4$ μs, repetition frequency of 10 kHz, and voltage of 0.6 kV peak–peak.

Finally, the ability of the converter to generate high repetition rate pulses only depends on the speed of the selected controller in executing the control software instructions, such that the total software execution time is less than the required pulse repetition time. For high repetition rates and/or short pulse durations, the utilization of fast (short turn ON delays) semiconductor switches is mandatory.

VIII. Conclusion

This paper presented a UPG, which emulates the dominate HV pulse waveforms in PEF electroporation applications. The proposed UPG topology is based on transition arms of series-connected HB-MMC cells, which has been utilized for quasi-two-level voltage generation in DAB dc–dc converters for HVDC transmission applications. In the UPG, two transition arms are used for negative and positive voltage pulse generation along with two bistate arms, which allow charging of the transition arms capacitors. The proposed UPG generates multilevel pulses that have low dv/dt, which allow reduction of the EMI generated by the converter. The controller software algorithm allows manipulation of the multilevel pulse-waveform characteristics to generate rectangular, exponential, and combined narrow and wide pulses. The UPG can generate both bipolar and monopolar HV pulse waveforms of microsecond pulse durations with controllable voltage magnitude, pulse duration, and pulse repetition frequency characteristics. Therefore, the proposed topology provides flexibility via its controller software algorithm, along with hardware modularity, scalability, and redundancy. The HB-MMC cell capacitors in the transition arms provide a controllable energy source, which charges from the

dc input supply and discharges across the load. The bistate arms allow charging of the HB-MMC cell capacitors in the transition arms from the dc input supply. Unlike the conventional HB-MMC used in HVDC transmission applications, the UPG converter has reduced footprint, weight, and cost by utilizing small cell capacitances in the HB-MMC and employing bistate arms. The cell-capacitor voltages are maintained around V_s/N by measuring their individual voltages, continuously, and applying a sorting and rotating algorithm. Simulations and experimental results confirm the viability of the proposed UPG, which promotes it for PEF application.

REFERENCES

[1] S. Y. Tseng, T. F. Wu, and M. W. Wu, "Bipolar narrow-pulse generator with energy-recovery feature for liquid-food sterilization," *IEEE Trans. Ind. Electron.*, vol. 55, no. 1, pp. 123–132, Jan. 2008.

[2] K. H. Schoenbach, F. E. Peterkin, R. W. Alden, and S. J. Beebe, "The effect of pulsed electric fields on biological cells: Experiments and applications," *IEEE Trans. Plasma Sci.*, vol. 25, no. 2, pp. 284–292, Apr. 1997.

[3] M. Rebersek and D. Miklavcic, "Advantages and disadvantages of different concepts of electroporation pulse generation," *Autom. J. Control, Meas., Electron., Comput. Commun.*, vol. 52, no. 1, pp. 12–19, 2011.

[4] K. H. Schoenbach, S. Katsuki, R. H. Stark, E. S. Buescher, and S. J. Beebe, "Bioelectrics—New applications for pulsed power technology," *IEEE Trans. Plasma Sci.*, vol. 30, no. 1, pp. 293–300, Feb. 2002.

[5] A. Sheikholeslami and J. Adabi, "High-voltage pulsed power supply to generate wide pulses combined with narrow pulses," *IEEE Trans. Plasma Sci.*, vol. 42, no. 7, pp. 1894–1901, Jul. 2014.

[6] A. Abou-Ghazala, S. Katsuki, K. H. Schoenbach, F. C. Dobbs, and K. R. Moreira, "Bacterial decontamination of water by means of pulsed-corona discharges," *IEEE Trans. Plasma Sci.*, vol. 30, no. 4, pp. 1449–1453, Aug. 2002.

[7] H. Bluhm, *Pulsed Power Systems: Principles and Applications*. Berlin, Germany: Springer, 2006.

[8] J. Raso and V. Heinz, *Pulsed Electric Fields Technology for The Food Industry: Fundamentals and Applications*. New York, NY, USA: Springer, 2006.

[9] Q. Bai-Lin, Z. Qinghua, G. V. Barbosa-Canovas, B. G. Swanson, and P. D. Pedrow, "Inactivation of microorganisms by pulsed electric fields of different voltage waveforms," *IEEE Trans. Dielectr. Elect. Insul.*, vol. 1, no. 6, pp. 1047–1057, Dec. 1994.

[10] W. Tsai-Fu, T. Sheng-Yu, and H. Jin-Chyuan, "Generation of pulsed electric fields for processing microbes," *IEEE Trans. Plasma Sci.*, vol. 32, no. 4, pp. 1551–1562, Aug. 2004.

[11] S. H. Jayaram, "Sterilization of liquid foods by pulsed electric fields," *IEEE Elect.. Insul. Mag.*, vol. 16, no. 6, pp. 17–25, Nov./Dec. 2000.

[12] M. S. Moonesan and S. H. Jayaram, "Effect of pulse width on medium temperature rise and microbial inactivation under pulsed electric field food treatment," *IEEE Trans. Ind. Appl.*, vol. 49, no. 4, pp. 1767–1772, Jul./Aug. 2013.

[13] H. Shi, Y. Lu, T. Gu, J. Qiu, and K. Liu, "High-voltage pulse-waveform modulator based on solid-state Marx generator," *IEEE Trans. Dielectr. Elect. Insul.*, vol. 22, no. 4, pp. 1983–1990, Aug. 2015.

[14] C. Yao, S. Dong, Y. Zhao, Y. Mi, and C. Li, "A novel configuration of modular bipolar pulse generator topology based on Marx generator with double power charging," *IEEE Trans. Plasma Sci.*, vol. 44, no. 10, pp. 1872–1878, Oct. 2016.

[15] J. Wu *et al.*, "A novel compact repetitive frequency square-wave generator based on coaxial pulse forming lines and coupled magnetic switches," *IEEE Trans. Plasma Sci.*, vol. 42, no. 6, pp. 1714–1720, Jun. 2014.

[16] L. Li, K. Liu, and J. Qiu, "Repetitive high voltage rectangular waveform pulse adder for pulsed discharge of capacitive load," *IEEE Trans. Dielectr. Elect. Insul.*, vol. 20, no. 4, pp. 1218–1223, Aug. 2013.

[17] E. Veilleux, B. T. Ooi, and P. W. Lehn, "Marx dc-dc converter for high-power application," *IET Power Electron.*, vol. 6, no. 9, pp. 1733–1741, Nov. 2013.

[18] T. Sakamoto, A. Nami, M. Akiyama, and H. Akiyama, "A repetitive solid state Marx-type pulsed power generator using multistage switch-capacitor cells," *IEEE Trans. Plasma Sci.*, vol. 40, no. 10, pp. 2316–2321, Oct. 2012.

[19] M. Rezanejad, A. Sheikholeslami, and J. Adabi, "Modular switched capacitor voltage multiplier topology for pulsed power supply," *IEEE Trans. Dielectr. Elect. Insul.*, vol. 21, no. 2, pp. 635–643, Apr. 2014.

[20] S. Zabihi, F. Zare, G. Ledwich, A. Ghosh, and H. Akiyama, "A new pulsed power supply topology based on positive buck-boost converters concept," *IEEE Trans. Dielectr. Elect. Insul.*, vol. 17, no. 6, pp. 1901–1911, Dec. 2010.

[21] A. Elserougi, A. M. Massoud, and S. Ahmed, "A modular high-voltage pulse-generator with sequential charging for water treatment applications," *IEEE Trans. Ind. Electron.*, vol. 63, no. 12, pp. 7898–7907, Dec. 2016.

[22] L. L. Rocha, J. F. Silva, and L. M. Redondo, "Multilevel high-voltage pulse generation based on a new modular solid-state switch," *IEEE Trans. Plasma Sci.*, vol. 42, no. 10, pp. 2956–2961, Oct. 2014.

[23] L. L. Rocha, J. F. Silva, and L. M. Redondo, "Seven-level unipolar/bipolar pulsed power generator," *IEEE Trans. Plasma Sci.*, vol. 44, no. 10, pp. 2060–2064, Oct. 2016.

[24] L. M. Redondo and J. F. Silva, "Flyback versus forward switching power supply topologies for unipolar pulsed-power applications," *IEEE Trans. Plasma Sci.*, vol. 37, no. 1, pp. 171–178, Jan. 2009.

[25] A. Elserougi, A. M. Massoud, A. M. Ibrahim, and S. Ahmed, "A high voltage pulse-generator based on DC-to-DC converters and capacitor-diode voltage multipliers for water treatment applications," *IEEE Trans. Dielectr. Elect. Insul.*, vol. 22, no. 6, pp. 3290–3298, Dec. 2015.

[26] I. A. Gowaid, G. P. Adam, B. W. Williams, A. M. Massoud, and S. Ahmed, "The transition arm multilevel converter— A concept for medium and high voltage dc-dc transformers," in *Proc. IEEE Int. Conf. Ind. Technol.*, 2015, pp. 3099–3104.

[27] F. Zare, "EMI issues in modern power electronic systems," *IEEE EMC Soc. Newslett.*, no. 221, pp. 66–70, 2009.

[28] G. P. Adam, O. Anaya-Lara, G. M. Burt, D. Telford, B. W. Williams, and J. R. McDonald, "Modular multilevel inverter: Pulse width modulation and capacitor balancing technique," *IET Power Electron.*, vol. 3, no. 5, pp. 702–715, Sep. 2010.

[29] A. Nami, L. Jiaqi, F. Dijkhuizen, and G. D. Demetriades, "Modular multilevel converters for HVDC applications: Review on converter cells and functionalities," *IEEE Trans. Power Electron.*, vol. 30, no. 1, pp. 18–36, Jan. 2015.

[30] M. A. Elgenedy, A. Darwish, S. Ahmed, and B. W. Williams, "A modular multilevel-based high-voltage pulse generator for water disinfection applications," *IEEE Trans. Plasma Sci.*, vol. 44, no. 11, pp. 2893–2900, Nov. 2016.

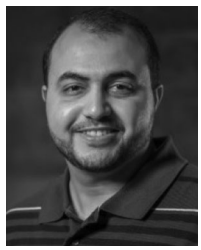

Mohamed A. Elgenedy (S'15) received the B.Sc. (with first-class honors) and M.Sc. degrees in electrical engineering from Alexandria University, Alexandria, Egypt, in 2007 and 2010, respectively. He is currently working toward the Ph.D. degree at the University of Strathclyde, Glasgow, U.K.

He is also an Assistant Lecturer with the Department of Electrical Engineering, Faculty of Engineering, Alexandria University. In 2012, he was as a Research Engineer with Spiretronic LLC, Houston, TX, USA. From 2013 to 2014, he was a Research Associate at Texas A&M University at Qatar. His research interests include high-power electronics, electric machine drives, energy conversion, and renewable energy.

Ahmed Darwish received the B.Sc. and M.Sc. degrees in electrical engineering from the Faculty of Engineering, Alexandria University, Alexandria, Egypt, in 2008 and 2012, respectively, and the Ph.D. degree in electric engineering from the Department of Electronic and Electrical Engineering, University of Strathclyde, Glasgow, U.K., in 2015.

From 2009 to 2012, he was a Research Assistant at Texas A&M University at Qatar, Doha, Qatar. He is currently a Research Associate with PEDEC Group at the University of Strathclyde. His research interests include dc–dc converters, multilevel converters, electric machines, digital control of power electronic systems, energy conversion, renewable energy, and power quality.

Shehab Ahmed (SM'12) was born in Kuwait City, Kuwait, in July 1976. He received the B.Sc. degree in electrical engineering from Alexandria University, Alexandria, Egypt, in 1999, and the M.Sc. and Ph.D. degrees from the in electrical and computer engineering from Texas A&M University, College Station, TX, USA, in 2000 and 2007, respectively.

From 2001 to 2007, he was with Schlumberger Technology Corporation working on downhole mechatronic systems. He is currently an Assoicate Professor with Texas A&M University at Qatar, Doha, Qatar. His research interests include mechatronics, solid-state power conversion, electric machines, and drives.

Barry W. Williams received the M.Eng.Sc. degree in electrical and electronic engineering from the University of Adelaide, Adelaide, Australia, in 1978, and the Ph.D. degree in electrical and electronic engineering from Cambridge University, Cambridge, U.K., in 1980.

After seven years as a Lecturer at Imperial College, University of London, London, U.K., he was appointed to a Chair of Electrical Engineering at Heriot-Watt University, Edinburgh, U.K., in 1986. He is currently a Professor at the University of Strathclyde, Glasgow, U.K. His teaching covers power electronics (in which he has a free internet text) and drive systems. His research activities include power semiconductor modeling and protection, converter topologies, soft-switching techniques, and application of application-specific integrated circuits and microprocessors to industrial electronics.